ACS OMEGA

Open Access

http://pubs.acs.org/journal/acsodf

Article

Deprotonation of 8-Oxo-7,8-dihydroadenine Radical Cation in Free and Encumbered Context: A Theoretical Study

Yinghui Wang,* Lei Ma, and Simin Wei*

Cite This: *ACS Omega* 2024, 9, 50730−50741

Read Online

ACCESS | Metrics & More | Article Recommendations | Supporting Information

ABSTRACT: Due to the lower oxidation potential than natural nucleic acid bases, one-electron oxidation of DNA is usually funneled into the direction of intermediates for oxidized DNA damage like 8-oxo-7,8-dihydroadenine (8-oxoA) leading to a radical cation, which may undergo facile deprotonation. However, compared to the sophisticated studies devoted to natural bases, much less is known about the radical cation degradation behavior of an oxidized DNA base. Inspired by this, a comprehensive theoretical investigation is performed to illuminate the deprotonation of 8-oxoA radical cation (8-oxoA$^{\bullet+}$) in both free and encumbered context by calculating the pK_a value and mapping the energy profiles. The calculative pK_a values of active protons in free 8-oxoA$^{\bullet+}$ follow the order: N7−H < N9−H < N6−H1< N6−H2, suggesting the preference of proton departure in free 8-oxoA$^{\bullet+}$. To further illustrate the preferred site and mechanism for 8-oxoA$^{\bullet+}$ deprotonation, energy profiles are constructed to distinguish the possibility from that of all active protons in both contexts. The results show distinctly that 8-oxoA$^{\bullet+}$ mainly suffers from the loss of proton from N9 due to the lowest energy barrier but deprotonates N7−H in real DNA as the connection of N9 and ribose. The energy barriers for the deprotonation of N7−H from 8-oxoA$^{\bullet+}$ in free and encumbered contexts are 1.5 and 1.3 kcal/mol, respectively, indicating a fast deprotonation reaction. It is more interestingly that the N9−H proton transfer (PT, toward N3) to adjacent water follows a stepwise fashion rather than a one-step approach as previously reported. Furthermore, the PT behavior of free N9−H toward O8 is dramatically influenced by base pairing T, where it is localized at neighboring water without further PT to adjacent water in free 8-oxoA$^{\bullet+}$ but migrated directly to adjacent water in the 8-oxoA$^{\bullet+}$:T base pair. And the deprotonation of N6−H2 in 8-oxoA$^{\bullet+}$:T is disturbed as the PT to O4 of the pairing T base is inhibited. It is warmly anticipated that these results could provide an in-depth perspective to understand the important role of 8-oxoA in mutation.

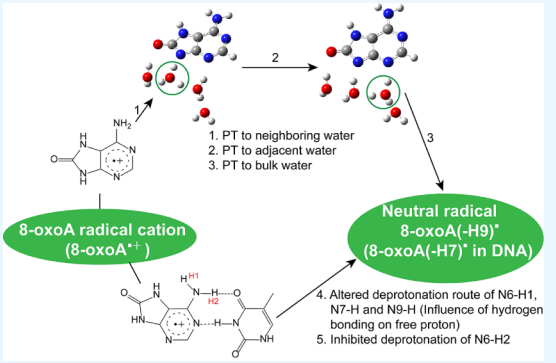

1. INTRODUCTION

Proton transfer (PT) has attracted continuous interest in both experimental and theoretical studies due to its ubiquity throughout chemistry and biology, for example, in proteins, enzymes, DNA, proton channels, and proton pumps.[1−9] Especially in DNA, the significance of PT has already been underlined since occasionally occurring in one of its less likely tautomeric forms may be implicated in spontaneous mutations.[10−12] The tautomer of a nucleotide incurring by PT differs from their canonical forms and could alter the correspondence of canonical base pair (AT/GC) leading to the mispairing of guanine (G) and thymine (T).[13] It is extremely destructive when the mispairing occurs at the time of DNA replication as the appearance of a substitution mutation in DNA sequence.[14,15] Apart from spontaneous point mutations, DNA is also susceptible to attack by external reactive oxygen species (ROS) or ionizing radiation resulting in mutational products like 8-oxo-7,8-dihydroguanine (8-oxoG) and 8-oxo-7,8-dihydroadenine (8-oxoA).[16−20] Normally, these mutational products could be removed by base excision repair pathway.[21−23] However, if the repair pathway is disturbed, it could cause mutations or cell death.[14,15,24−26] It is universally acknowledged that the degradation of DNA to mutational products after reacting with external reagents involves PT at various stages.[18,27−31] Evidently, illustrating the mechanism of PT in DNA has significant importance for the point mutations, although the relationship between PT and mutation is still controversial.

One of the most potent sources of cytotoxic DNA lesions related to mutagenesis is the one-electron oxidation of nucleobases, which usually occurs after the exposure of DNA to ionizing radiation or photosensitizers.[18,32−36] Evidence is now accumulating that one-electron oxidation of DNA would initially generate a radical cation and ultimately ends up

Received: September 30, 2024
Revised: December 2, 2024
Accepted: December 6, 2024
Published: December 13, 2024

selectively at the site of G leading to the guanine radical cation ($G^{\bullet+}$) due to the lowest oxidation potential.[37−40] Subsequently, the $G^{\bullet+}$ would mainly undergo facile PT usually termed as deprotonation.[41−43] Thus, the deprotonation of $G^{\bullet+}$ in different DNA contexts has been extensively studied. For example, by nanosecond laser flash photolysis, the deprotonation behavior of $G^{\bullet+}$ within G-quadruplexes was observed directly, which is mainly loss of amino proton (N2−H) instead of imino proton (N1−H) and is slower (1−2 orders of magnitude) than the case in free G or duplex DNA.[41] And the formation mechanisms of intermediates in one-electron oxidized G-quadruplex were unraveled by calculating the relative Gibbs free energies, spin density distributions, and its various proton-transfer states in a G-quartet.[44] The structural effects on the reactivity of $G^{\bullet+}$ were also clarified by studying the $G^{\bullet+}$ reaction dynamics in triplex DNA using time-resolved spectroscopy and Fourier transform infrared characterization of steady-state products.[42]

In comparison to natural nucleic acid bases, some intermediates for oxidized DNA damage have lower oxidation potential due to the subtle changes in electronic properties such as 8-oxoG (0.74 V *vs.* NHE). Experimental observation has verified that the oxidation of DNA is funneled into the direction of 8-oxoG hinting at the preference of hole trap in DNA embedded with it.[39,45] Studies have postulated that after further oxidation of 8-oxoG by extracting one electron, 8-oxoG radical cation (8-oxoG$^{\bullet+}$) could be primarily generated, which then deprotonates N7−H to form a neutral radical (8-oxoG(N7−H)$^{\bullet}$) in both free and constrained context.[28,46,47] The fate of 8-oxoG(N7−H)$^{\bullet}$ are the mutable stereoisomers of guanidinohydantoin (Gh) and spiroiminodihydantoin (Sp).[48,49] It is obvious that the study on the deprotonation of an oxidative base has its biological significance.

8-oxoA is a prominent product of adenine (A) oxidation by reactive oxygen species like hydroxyl radicals and one-electron oxidant, and has been discerned in living mammals after γ-irradiation, where increased levels of 8-oxoA were detected in human cancers.[50,51] In vivo, 8-oxoA is weakly mutagenic, but it prefers to cause A → C and A → G substitutions indicating the transient formation of 8-oxoA:G and 8-oxoA:C mispairing.[14,15,24,25] 8-oxoA is composed of a purine ring containing a carbonyl group and an exocyclic amine at the C8 and C6 positions, respectively. Owing to the unique electronic properties, the oxidation potential of 8-oxoA (0.89 V *v.s* NHE) is much lower than A (1.42 V *v.s* NHE) and G (1.29 V *v.s* NHE), suggesting a far more reactivity than the natural nucleic acid bases and the preference to react with one-electron oxidant generating 8-oxoA radical cation (8-oxoA$^{\bullet+}$). However, to the best of our knowledge, only Peter O'Neill and his coworkers monitored the decay of 8-oxoA$^{\bullet+}$, which referred to the formation of N6-centered radical (8-oxoA(−H6)$^{\bullet}$) after reacting with $N_3^{\bullet}$ within 11 μs at pH 7.0, suggesting a fast deprotonation from N6 (Scheme 1).[52] To carefully check the structure of 8-oxoA, both imino (N7−H) and amino protons (N6−H) are involved, where the acidity of the former is generally stronger than the latter in the form of both neutral and radical cations. The acidity analysis seems to be contrary to the experimental result. Furthermore, study indicated that in duplex DNA, 8-oxoA is paired with thymine (T) via two hydrogen bonds similar to A:T base pair (Scheme 1).[24] This means that the most favorable site of 8-oxoA$^{\bullet+}$ deprotonation referred to in the literature may be occupied. The study of hydrogen bonding effects appears to be essential to elucidate

Scheme 1. Degradation of 8-oxoA$^{\bullet+}$ at Initial Stage in the Literature and the Main Purpose of This Work

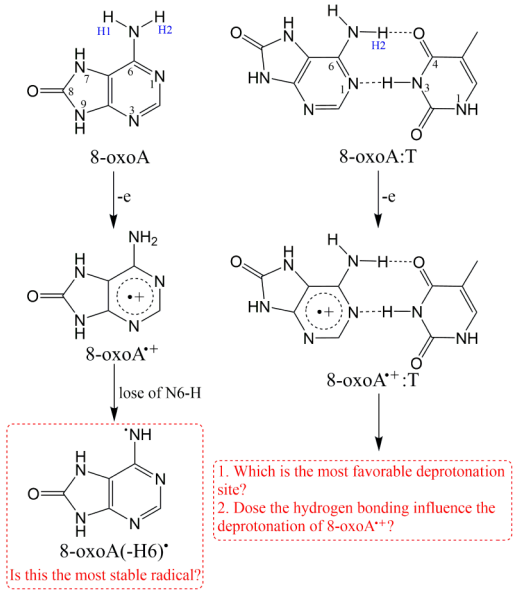

the degradation mechanism of 8-oxoA$^{\bullet+}$ in a DNA context. However, the formation and degradation of 8-oxoA$^{\bullet+}$ in DNA context remain elusive to a large extent in a previous study.[52] Obviously, further study should be performed to disclose the ambiguous mechanism of 8-oxoA$^{\bullet+}$ deprotonation in various contexts.

Inspired by these, a thorough theoretical investigation was implemented to illustrate the mechanism of 8-oxoA$^{\bullet+}$ deprotonation in free and encumbered context. To render an insightful view, the thermodynamic properties of the reaction are uncovered by calculating the pK_a value of active protons in its free form, which initially sheds light on the preference of proton departure. Then, the kinetic properties of active protons in free 8-oxoA$^{\bullet+}$ are assessed to illuminate the realizability of deprotonation from these sites and supply an ideal reference to expose the influence of hydrogen bonding in 8-oxoA$^{\bullet+}$ deprotonation. The most possible neutral radical deriving from 8-oxoA$^{\bullet+}$ deprotonation is distinctly indicated after carefully inspecting both the pK_a values and energy profiles rationalizing the previous experimental result. With these innovative results, it is easy to discern the possible site of 8-oxoA$^{\bullet+}$ deprotonation in a single-layer base pair. The inherent effect of hydrogen bonding on 8-oxoA$^{\bullet+}$ deprotonation is unraveled, which could alter the deprotonation behavior even for free proton. This result makes the influence of hydrogen bonding on DNA radical cation deprotonation more comprehensive. It is warmly anticipated that these results could shed light on the elusive degradation for oxidized DNA base.

2. RESULTS AND DISCUSSION

2.1. The pK_a of 8-oxoA$^{\bullet+}$. Since the pH-dependent fashion of deprotonation reaction, the pK_a of individual nucleosides is an important factor for clarifying the deprotonation mechanism of DNA radical cation. Thus, the pK_a of active protons in 8-oxoA$^{\bullet+}$ tends to be predicted at the M06-2X/6-31+(d,p) level of theory, where the solvation effect is simulated by integral equation formalism-polarized continuum model (IEFPCM) augmented with seven explicit water molecules. This disposal has acquired improvements in

https://doi.org/10.1021/acsomega.4c08956
ACS Omega 2024, 9, 50730−50741

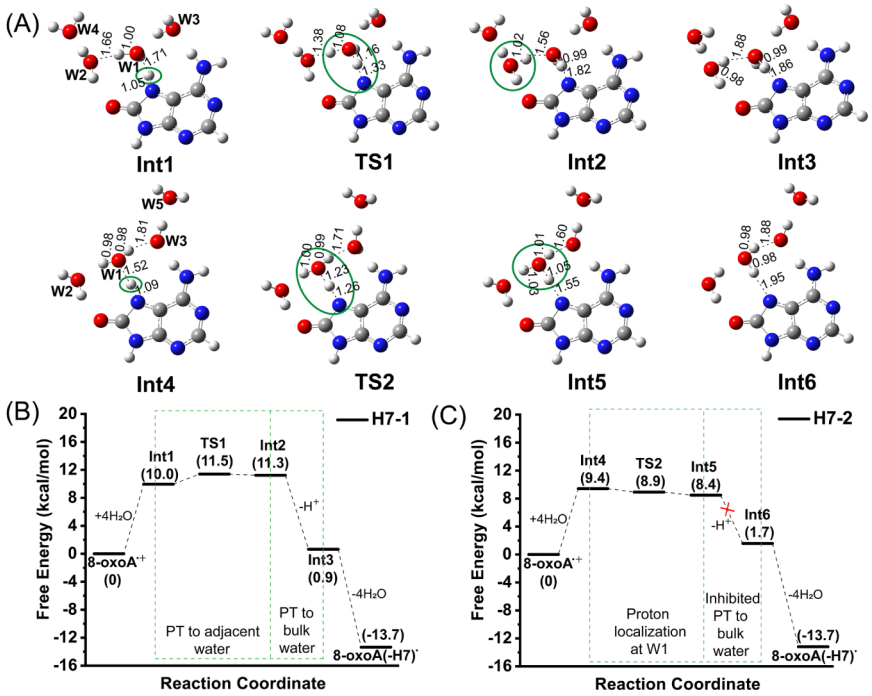

Figure 1. (A) Optimized geometries and Gibbs energy profiles of (B) H7−1 and (C) H7−2 pathway.

predicting pK_a in other DNA bases.[46,53] The explicit water molecules are mainly placed around N1, N3, N6−H, N7−H, and O8 and N9 in related species involved in the deprotonation reaction. To rationalize the methodology, the pK_a of active proton was initially calculated in 8-oxoA due to the referable value of N7−H (8.7). Herein, the calculated pK_a value of N7−H is 9.2 with 0.5 deviation in comparison with the experimental value, indicating the applicability of the treatment. Actually, the influence of density functional theory (DFT) and solvation was also evaluated, which revealed greater deviations related to experimental value (see Table S1). Incidentally, the pK_a values of N6−H1, N6−H2, and N9−H were then disclosed to be 17.2, 17.1, and 9.4, respectively. The acidity of active protons in 8-oxoA is in the order: N7−H > N9−H > N6−H2 > N6−H1. It is clear that N7−H is the most acidic position in 8-oxoA approving the above-mentioned statement.

Subsequently, the pK_a values of active protons in 8-oxoA$^{\bullet+}$ were obtained to be −6.1, −1.5, 0.6, and 1.6, respectively, following the order: N7−H < N9−H < N6−H1 < N6−H2. It seems fallacious due to the appearance of negative pK_a values. We speculated that this may originate from the strong acidity of N7−H and N9−H corresponding to the high stabilization energy of 8-oxoA(−H7)$^{\bullet}$ and 8-oxoA(−H9)$^{\bullet}$. The negative pK_a values are also found when other combination of DFT and solvation model was adopted, such as SMD/B3LYP, IEFPCM/CAM-B3LYP, and IEFPCM/WB97XD, with a similar basis set. In all related calculations, the acidity follows similar order to that obtained at the IEFPCM/M06−2X/6−31+(d,p) level of theory. Although the accurate pK_a value of active protons in 8-oxoA$^{\bullet+}$ could not be disclosed, this result manifests the dramatically increased acidity of 8-oxoA$^{\bullet+}$ in comparison with 8-oxoA and suggests the tendency of 8-oxoA$^{\bullet+}$ deprotonation even in a strong acid aqueous solution. This agrees well with the previous experimental result, and is basically similar to 8-oxoG$^{\bullet+}$, which could deprotonate to form a neutral radical 8-oxoG(−H7)$^{\bullet}$ at pH 3.0.[47]

2.2. The Deprotonation of 8-oxoA$^{\bullet+}$ in Free Context.

The deprotonation of DNA radical cation in unencumbered context mainly proceeds the PT to adjacent water, following the PT to bulk water, hinting at the significance of adjacent water. Previous studies on the G$^{\bullet+}$ deprotonation showed that at least four explicit waters are required for stimulating the deprotonation reaction, and the important role of water in the second hydration layer and the water in the opposite direction of PT is emphasized.[54,55] Thus, to mimic the 8-oxoA$^{\bullet+}$ deprotonation properly, four explicit water molecules are introduced around the site of active proton in all models as in a previous study.[54] Moreover, the potential of PT to various directions is intended to be elucidated by adjusting the orientation of hydrogen-bonded O−H in neighboring water of the active proton. The possible reaction pathway for 8-oxoA$^{\bullet+}$ deprotonation was then carefully examined, where 8-oxoA$^{\bullet+}$ and four water molecules are used as the reference of zero energy. The optimized geometries of 8-oxoA, 8-oxoA$^{\bullet+}$, and the neutral radicals are displayed in Figure S1.

As the strongest acidity of N7−H, the possibility for the deprotonation of N7−H was first assessed by mapping the profiles of Gibbs free energy. The reaction begins with the water coordination to N7−H, N6−H1, and O8 of 8-oxoA$^{\bullet+}$, where an extra water was added in the second hydration shell to aid the proton migration to bulk water as in a previous study.[54] These four water molecules are denoted as W1, W3, W2, and W4/W5, respectively. It is anticipated that the N7−H of 8-oxoA$^{\bullet+}$ could be initially transferred toward the O8 or N6−H pathway termed as H7−1 and H7−2 pathways, respectively. As shown in Figure 1A, in the H7−1 pathway, one of the O−H bonds in W1 directs to W2, but in the H7−2 pathway, the two O−H bonds of W1 connect with both W2 and W3. It is the arrangement of W1 that may facilitate the proton transfer to O8 or N6−H. Noteworthily, the arrangement of W1 also guides the water position in the second hydration shell and in the opposite direction of PT. As shown in Figure 1B,C, the water coordination to 8-oxoA in the H7−1

https://doi.org/10.1021/acsomega.4c08956
ACS Omega 2024, 9, 50730−50741

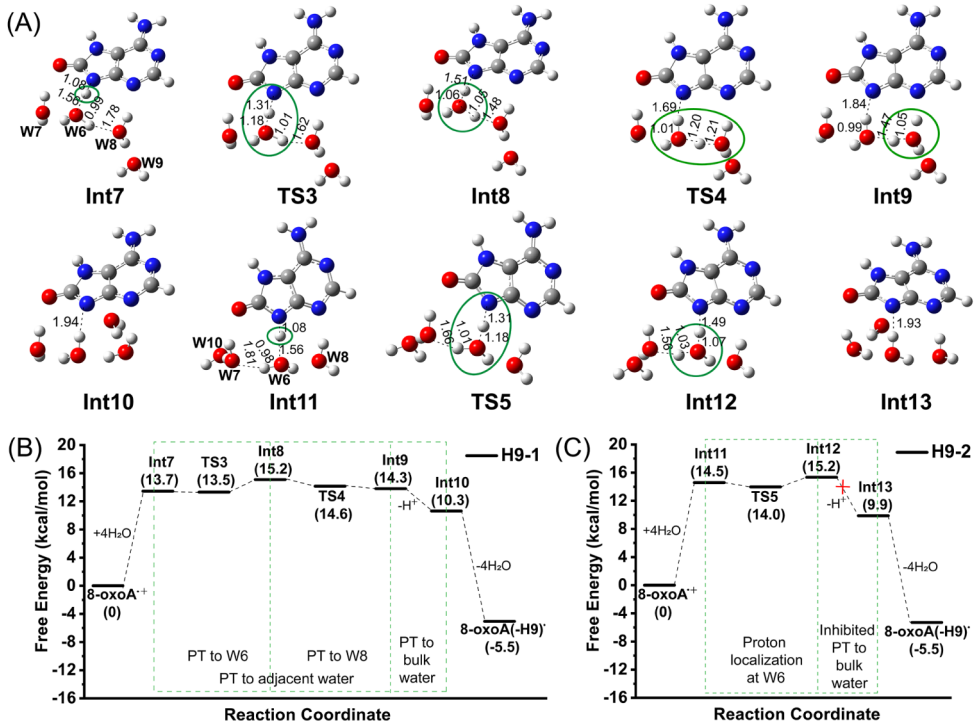

Figure 2. (A) Optimized geometries and Gibbs energy profiles of (B) H9−1 and (C) H9−2 pathway.

and H7−2 pathways is featured as destabilization of Int1 and Int4 with 10.0 and 9.4 kcal/mol energy acquisition, where the enthalpy change is −26.2 and −27.0 kcal/mol, respectively (Table S2). The energetic Int1 and Int4 with slightly elongated N7−H bond would migrate the N7−H to neighboring water forming Int2 and Int5 via TS1 and TS2 with forward energy barrier 1.5 and −0.5 kcal/mol, respectively. In both TS1 and TS2, the proton retains between N7 of 8-oxoA$^{\bullet+}$ and the O of W1 leading to the transient H_3O^+ at W1 in both pathways, where the N7−H bond would be further elongated. It is noticed that the O−H bond length of W1 in TS1 increases but remains largely unchanged in TS2. This difference may drive the proton migration with various fashion confirmed by checking the optimized structure of Int2 and Int5. Int2 features as the full cleavage of N7−H bond accompanying with the PT to W2. This is considered to be decisive for the deprotonation of DNA radical cation since the protonated W2 links with the water in second hydration layer and would migrate the proton further to bulk water.[54] Nevertheless, the proton is still limited to W1 in Int5, hinting at the disruption of proton transfer to bulk water even though the proton has escaped from N7 with negligible energy barrier (−0.5 kcal/mol). The energy scan along the O−H bond of W1 was performed to further certify this, where the energy increases continuously with the enhanced length of the O−H bond (Figure S2). It supposes that it may derive from the saturability of hydrogen bonding in W3. This means that the N7−H may follow the H7−1 pathway to form a neutral radical as the inaccessible H7−2 pathway. The proton escapes from N7 to neighboring water along with H7−1 and H7−2 pathways, which also reveals different thermodynamic properties, where Int2 is 1.3 kcal/mol less stable than Int1, but Int5 is 1.0 kcal/mol more stable than Int4. Noticeably, Int2 is not pure neutral radical 8-oxoA-(−H7)$^{\bullet}$, where the escaped proton should be further migrated to bulk water along with the water network. It is known that PT in water network has an abnormally high transport efficiency (1−2 ps at room temperature).[56] Thus, the PT of bulk water was not monitored in the calculations. The whole deprotonation of Int2 imparts 10.4 kcal/mol energy on Int3. After the dissociation of four waters, the sole 8-oxoA(−H7)$^{\bullet}$ could be generated, which is 13.7 kcal/mol more stable than 8-oxoA$^{\bullet+}$ indicating the exothermic nature. Herein, the calculative result of 8-oxoA$^{\bullet+}$ deprotonation is basically similar to other DNA base reported in previous studies, where W1 plays the role of proton bridge and the departing proton is temporarily localized at W2 ready to migration to bulk water.[36,46,54]

Then, the energy profiles of loss of N9−H were explored, where the extra waters are located around N9−H, O8, and N3 denoted as W6, W7, and W8 instead of W1, W2, and W3, respectively. The water in the second hydration shell (W9/W10) is added based on the direction of O−H bond in W6. In the H9−1 pathway, the outer water (W9) connects with W8 by hydrogen bonding and the direction of PT is expected to be N3. However, in the H9−2 pathway, W10 is placed around W7, indicating that the proton may migrate toward the direction of O8. Figure 2A exhibits the optimized structures of water-coordinated 8-oxoA$^{\bullet+}$ in H9−1 (Int7) and H9−2 pathway (Int11). As displayed in Figure 2B,C, both Int7 and Int11 are 13.7 and 14.5 kcal/mol less stable than sole 8-oxoA$^{\bullet+}$, indicating the endothermic nature of water coordination reaction consistent with the case in H7−1 and H7−2 pathway. The lengths of the N9−H bond in both Int7 and Int11 are slightly elongated, revealing the tendency of proton escape from N9. Similar to the case in H7−1 and H7−2 pathways, the temporary H_3O^+ was also detected in the neighboring water of active proton (N9−H) in TS3 and TS5. Int7 and Int11 are 0.2 and 0.5 kcal/mol less stable than TS3 and TS5, but are 1.5 and 0.7 kcal/mol more stable than Int8 and Int12, respectively. This indicates the feature of negative

https://doi.org/10.1021/acsomega.4c08956
ACS Omega 2024, 9, 50730−50741

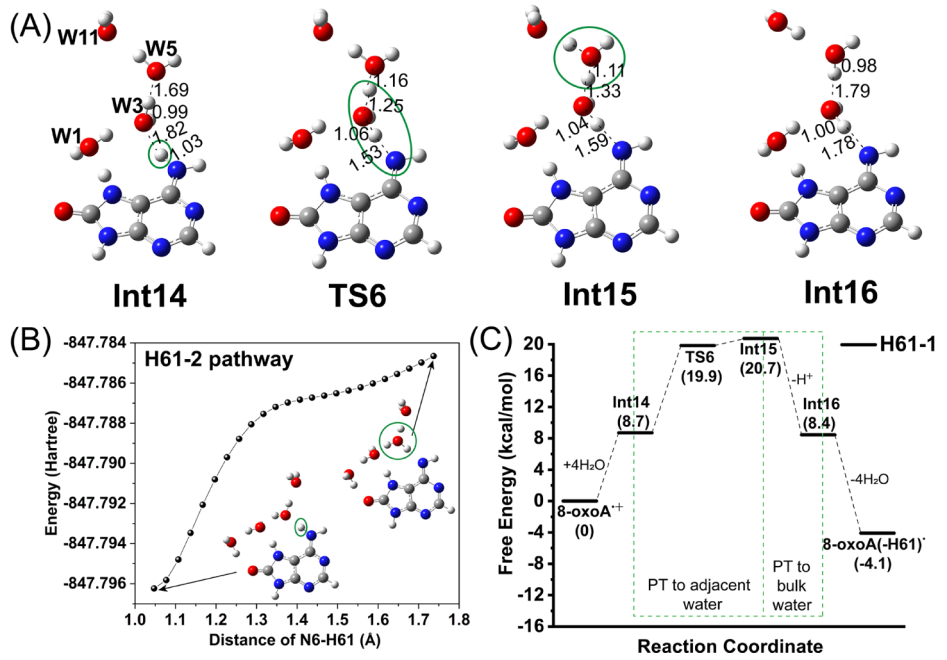

Figure 3. (A) Optimized geometries; (B) total energy scan of N6−H1 bond in the H61−2 pathway; and (C) Gibbs energy profile of the H61−1 pathway.

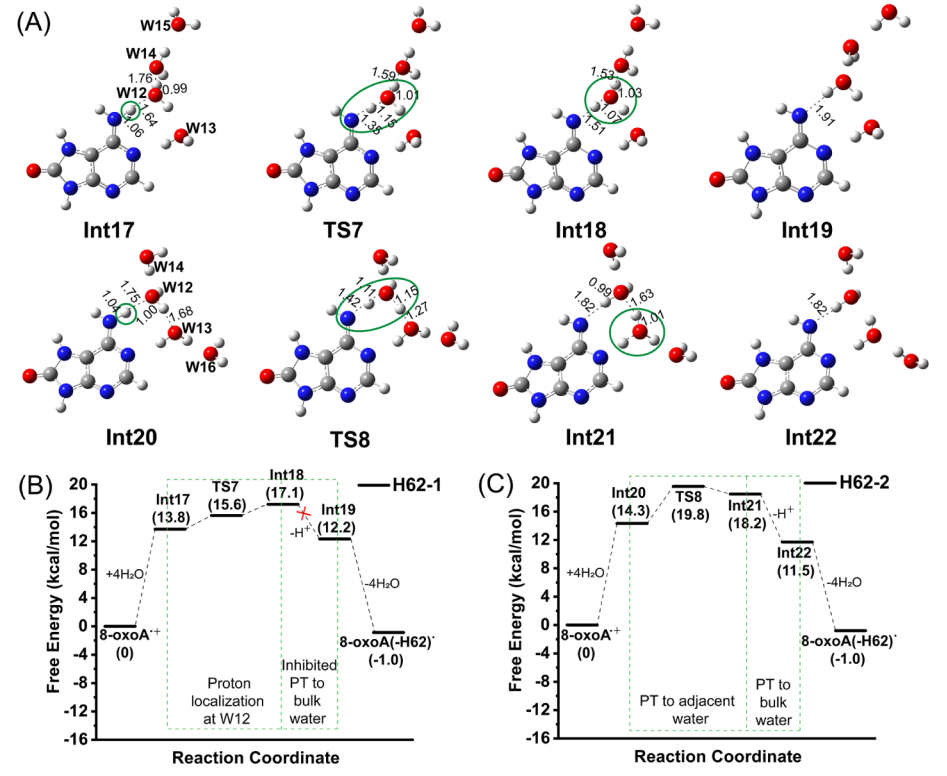

Figure 4. (A) Optimized geometries and Gibbs energy profiles of (B) H62−1 and (C) H62−2 pathway.

energy barrier and endothermic nature of proton escape to neighboring water. In both Int8 and Int12, the proton is located at W6 without further migration along the water network as in the case of the H7−2 pathway. Surprisingly, in the H9−1 pathway, the localized proton in Int8 could undergo a facile PT to W8 leading to the formation of decisive intermediate (Int9) via TS4. In TS4, a proton stays between W6 and W8, which is eventually stabilized at W8 in Int9. However, it is infeasible to transfer the localized proton in Int12 due to the absence of a stable product (Figure S3). This means that PT to bulk water along H9−2 pathway is disturbed, leading to an incomplete deprotonation of N9−H. The migration of H9 to adjacent water occurs in a stepwise fashion (two steps), which is dramatically different from the case of N7 of 8-oxoA$^{\bullet+}$ and other DNA radical cation (one step).[36,46,54]

https://doi.org/10.1021/acsomega.4c08956
ACS Omega 2024, 9, 50730−50741

Scheme 2. Degradation of 8-oxoA$^{\bullet+}$ to 8-oxoA(-H)$^{\bullet}$ via Different Pathways

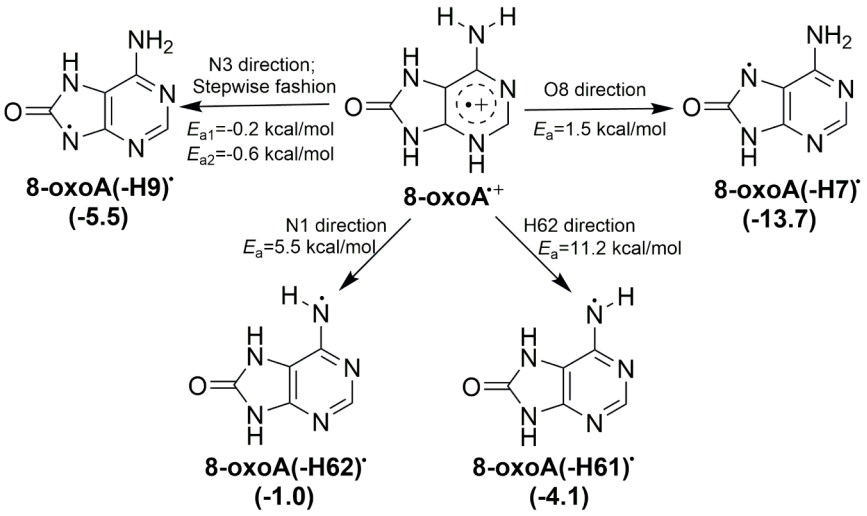

The possibility for loss of amino proton from 8-oxoA$^{\bullet+}$ was then studied by mapping the energy profile of deprotonated N6−H1 and N6−H2. Initially, the hydration model of the H7−2 pathway is adopted after slightly adjusting the direction of the O−H bond in neighboring water to facilitate the deprotonation of N6−H1 (H61−2 pathway, Figure 3B). Unexpectedly, after enormous efforts, a proper structure of TS is not detected, indicating the unfeasible deprotonation with the hydration model. To further confirm this, the total energy scan along with the N6−H1 bond is performed, which manifests a continuously increased energy, suggesting the absence of TS and a stable product (Figure 3B). Then, to build a proper hydration model for deprotonation N6−H1, W1, W3, and W5 are retained, and W2 is replaced by W11, which connects with W5 by hydrogen bonding, as shown in Figure 3A. With this hydration model, both the proton escape to neighboring water and the tendency of PT to bulk water are detected. In Int14, the N6−H1 bond is slightly activated by endothermic water coordination to 8-oxoA$^{\bullet+}$. With the cleavage of the N6−H1 bond, H_3O^+ is discerned in TS6 following a further proton migration to W5 to form the product of proton escape (Int15). This reaction is endothermic to be 12.0 kcal/mol with a forward energy barrier of 11.2 kcal/mol (Figure 3C). This is higher than the loss of H7 (1.5 kcal/mol) and H9 (−0.2 kcal/mol) in H7−1 and H9−1 pathways, hinting at the preference of 8-oxoA$^{\bullet+}$ deprotonation. The sole 8-oxoA(−H61)$^{\bullet}$ is 4.1 kcal/mol more stable than 8-oxoA$^{\bullet+}$, meaning an exothermic nature of deprotonation reaction similar to the energetics of loss of imino proton.

The exploration of 8-oxoA$^{\bullet+}$ deprotonation from N6−H2 was performed using the above-mentioned method, where four subtle water molecules are strategically introduced to build the H62−1 and H62−2 pathways (Figure 4). In the H62−1 pathway, two waters are first located around N6−H2 and N1 denoted as W12 and W13, where another two waters (W14 and W15) are hydrogen bonding with each other and W14 connects with W12. This strategy could ensure the occurrence of a complete 8-oxoA$^{\bullet+}$ deprotonation and the energetics. However, in the H62−2 pathway, W12, W13, and W14 still remained, but W15 is substituted with W16, which links with W13 by hydrogen bonding to induce the PT to outer water. Surprisingly, only the proton escape along the H62−1 pathway is discerned, where the escaped proton mainly localizes in W12. This could be reinforced by inspecting the optimized structures of related species in the H62−1 pathway (Figure 4A) and the total energy scan of the O−H bond in W12 (Figure S4). In Int17, four additional waters are arranged in order around N6−H2, which slightly activates the N6−H2 bond with an elongated length and less stability (13.8 kcal/mol, Figure 4B). As the reaction continues, the distance of N6···H2 increases continuously, indicating the proton departure from N6. Along the pathway, both the transition state (TS7) and intermediated product (Int18) could be captured readily, in which H_3O^+ is observed in W12 without any further migration to outer water. The reaction of proton departure from N6 along the H62−1 pathway is endothermic to be 3.3 kcal/mol with forward energy barrier 1.8 kcal/mol. However, the interrupted PT to outer water causes the infeasibility of deprotonation along the H62−1 pathway.

The accessibility of loss of N6−H2 from 8-oxoA$^{\bullet+}$ was validated by establishing the energy profile of the H62−2 pathway. After the endothermic water coordination to 8-oxoA$^{\bullet+}$, the formed Int20 could transfer the N6−H2 to W13 eventually, resulting in the product of proton escape (Int21) via TS8. The H_3O^+ occurs in W12 of TS8 temporarily and then migrates to W13 in Int21, indicating the role of the proton bridge of W12 and the trend of PT to outer water. Both TS8 and Int21 are 5.5 and 3.9 kcal/mol more stable than Int20, respectively, implying the forward energy barrier and the thermodynamics. The complete deprotonation of 8-oxoA$^{\bullet+}$ could be accomplished after the PT to bulk water and the dissociation of coordinated water, which are exothermic by 6.7 and 12.5 kcal/mol, respectively.

Herein, eight pathways are built to thoroughly uncover the 8-oxoA$^{\bullet+}$ deprotonation from four active sites, where only H7−1, H9−1, H61−1, and H62−2 pathways undergo an intact deprotonation (Scheme 2). This implies that the active protons may depart along these four paths. After careful inspection of the energy profiles, the favorable pathway of 8-oxoA$^{\bullet+}$ deprotonation could be ascertained to be the H9−1 pathway attributed to the lowest energy barrier (−0.5 kcal/mol). However, due to the linkage between N9 and ribose, N9−H did not exist in real DNA leading to the impossibility of 8-oxoA$^{\bullet+}$ deprotonation from N9. It is clear that the 8-oxoA$^{\bullet+}$

https://doi.org/10.1021/acsomega.4c08956
ACS Omega 2024, 9, 50730−50741

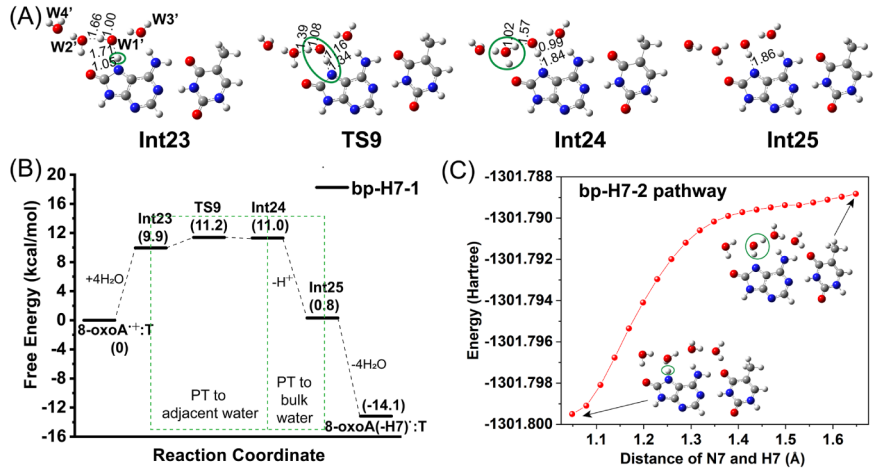

Figure 5. (A) Optimized geometries; (B) Gibbs energy profile of bp−H7−1 pathway; and (C) total energy scan of N7−H7 bond to neighboring water (W1′).

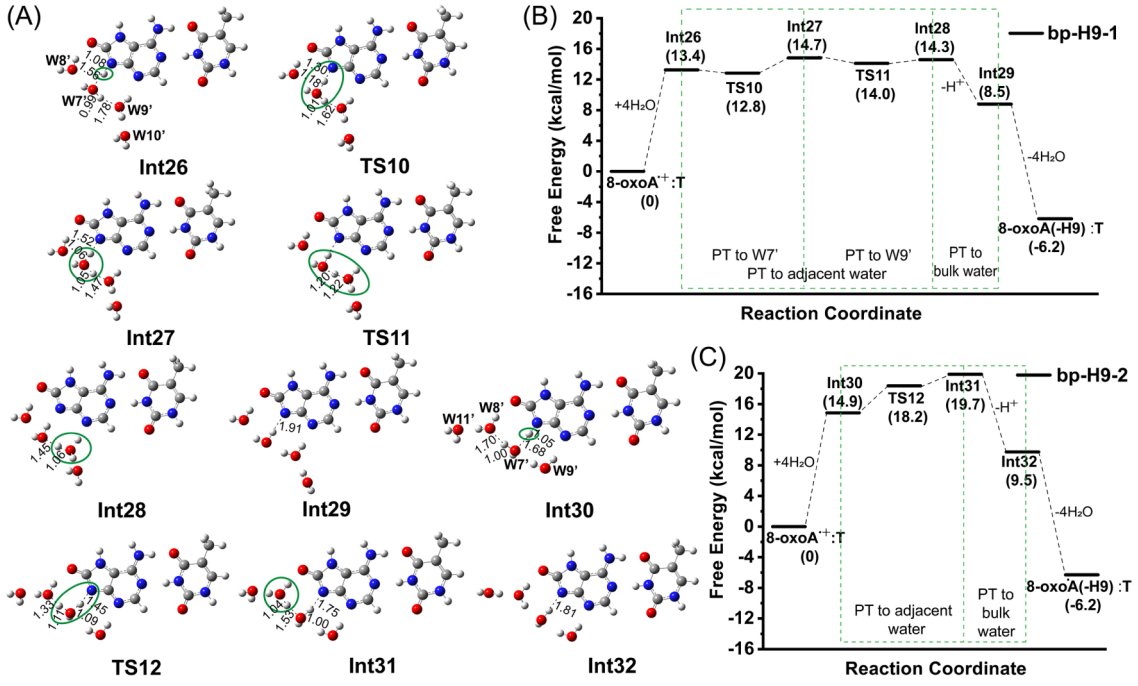

Figure 6. (A) Optimized geometries and the Gibbs energy profiles of (B) bp−H9−1 and (C) bp−H9−2 pathway.

would deprotonate from N7 along the H7−1 pathway. The energy barrier of deprotonation N7−H is also rather low (1.5 kcal/mol) verifying previous experimental result that the neutral radical formed within 11 μs.[52] It is noteworthy that 8-oxoA$^{\bullet+}$ deprotonation could also proceed along the H61−1 and H62−2 pathways with forward energy barriers of 11.2 and 5.5 kcal/mol, respectively. It is predictable that the H61−1 and H62−2 pathways may become important if the H7−1 pathway is inhibited. It should be also mentioned that in other pathways except for the H61−2 pathway, the active protons could escape from 8-oxoA$^{\bullet+}$ and are eventually localized at neighboring water. Considering the high instability of proton departed product, the reactions are infeasible along these pathways even though with negative energy barrier.

Otherwise, the stability of the neutral radical could be obtained, which follows the order: 8-oxoA(−H7)$^{\bullet}$ > 8-oxoA(−H9)$^{\bullet}$ > 8-oxoA(−H61)$^{\bullet}$ > 8-oxoA(−H62)$^{\bullet}$. Clearly, the most stable radical is 8-oxoA(−H7)$^{\bullet}$ verifying the identity of observed radical in a previous experimental study, which indicated the formation of 8-oxoA(−H6)$^{\bullet}$.[52]

2.3. The Deprotonation of 8-oxoA$^{\bullet+}$ in a Base Pair. According to previous studies,[18,41,42] if the DNA base is in encumbered context, the degradation pathway may alter, where the active sites are usually occupied by pairing with another base. Thus, the deprotonation reaction of 8-oxoA$^{\bullet+}$ is assessed in a single-layer 8-oxoA:T base pair to reveal the importance of hydrogen bonding, although the preferential site remains to be unencumbered. The strategy for water introduction is completely similar to the case in free 8-oxoA$^{\bullet+}$ with the superscript comma to distinguish them at different context, but the reference of zero energy is the 8-oxoA$^{\bullet+}$:T and four water molecules. The optimized structures of 8-oxoA:T, 8-oxoA$^{\bullet+}$:T, and the constrained neutral radicals are exhibited in Figure S5. There is only one active proton

https://doi.org/10.1021/acsomega.4c08956
ACS Omega 2024, 9, 50730−50741

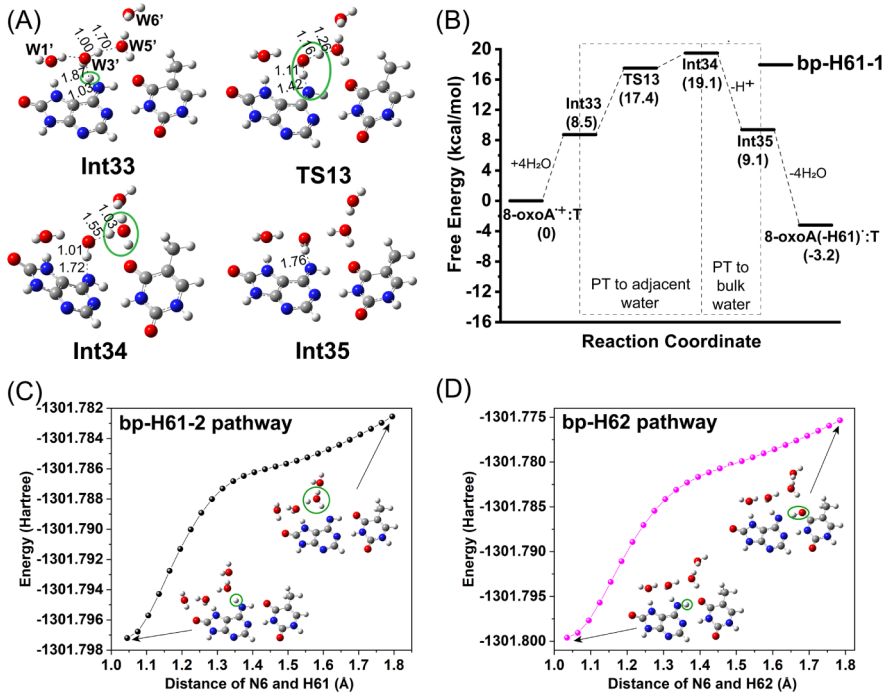

Figure 7. (A) Optimized geometries; (B) Gibbs energy profile of bp−H61−1 pathway; total energy scan of (C) N6−H1 bond to neighboring water (W3′) and (D) N6−H2 bond to paired T base.

(N6−H2) involved in hydrogen bonding offering another possible deprotonation path like G in the G:C base pair (see below).

Due to the priority of deprotonation of N7−H and N9−H in free 8-oxoA$^{\bullet+}$, an exploration for the case in a base pair was first implemented. As shown in Figure 5A,C, the hydration models adopted in the H7−1 and H7−2 pathways for free 8-oxoA$^{\bullet+}$ are employed to simulate the deprotonation N7−H of 8-oxoA$^{\bullet+}$:T termed the bp−H7−1 and bp−H7−2 pathway, respectively. Similar to free 8-oxoA$^{\bullet+}$, the introduction of four waters makes the 8-oxoA$^{\bullet+}$:T more vitality charactered as the elongated N7−H bond and the higher energy in Int23 (bp−H7−1 pathway, Figure 5B). This facilitates the departure of active proton from N7 to form Int24 via TS9, which is endothermic to be 1.1 kcal/mol with a forward barrier of 1.3 kcal/mol. The energy barrier is slightly lower than the case in free 8-oxoA$^{\bullet+}$ (1.5 kcal/mol), which may originate from the slight withdrawal of electron to paired T base. The comparison of the charge localized at the N7 site and at the O of water reinforces the speculation, which is −0.646 |e| and −0.645 |e| at N7, and −1.225 |e| and −1.222 |e| at the O of water in free and constrained 8-oxoA$^{\bullet+}$, respectively. The PT to bulk water would endow 10.2 kcal/mol stability on Int25 and the following water dissociation makes the step down to the most stable 8-oxoA(−H7)$^{\bullet}$:T. It appears that the energy barrier and the thermodynamics of proton departure to adjacent water is basically similar in both free and encumbered 8-oxoA$^{\bullet+}$.

The deprotonation of 8-oxoA$^{\bullet+}$:T from N7−H along the bp−H7−2 pathway was then evaluated. Interestingly, the analogous product of water coordination was not obtained, where W5′ is close to O4 of paired T base and hydrogen bonding with T in optimized structure. The absence of outer water may lead to the suspension of PT to bulk water. Surely, the TS of proton escape to neighboring water is unavailable. This is reinforced by the total energy scan of the N7−H bond of the optimized reactant, where the energy continuously increases meaning the absence of TS and a stable product (Figure 5C). It has a dramatic difference on the PT directed to the N6 site of 8-oxoA$^{\bullet+}$ in free and base pairing context. Obviously, the constrained context has an influence on the 8-oxoA$^{\bullet+}$ deprotonation even though for free proton, that supplements the conclusion of the effects of hydrogen bonding on the degradation for oxidative DNA base.

Then, the deprotonation of 8-oxoA$^{\bullet+}$:T from N9 was investigated by constructing the pathways of bp−H9−1 and bp−H9−2, where the hydration models were analogous to that in H9−1 and H9−2 pathway for free 8-oxoA$^{\bullet+}$. As shown in Figure 6, the N9−H departure from 8-oxoA$^{\bullet+}$:T could proceed directly along the bp−H9−2 pathway but follows a stepwise fashion in the bp−H9−1 pathway. It is with difference on the case in free 8-oxoA$^{\bullet+}$, where N9−H is stabilized at the neighboring W7 along the H9−2 pathway. Evidently, the encumbered context alters the migration route of free active proton again. Figure 6B,C displays the energy profile for the reaction along the bp−H9−1 and bp−H9−2 pathways. The reaction of proton localization in the bp−H9−1 pathway is endothermic to be 1.3 kcal/mol with a negative energy barrier (−0.6 kcal/mol) following a facile PT from W7′ to W9′ with energy barrier −0.7 kcal/mol. In comparison with the stepwise proton departure, the loss of proton along the bp−H9−2 pathway has a higher forward energy barrier (4.3 kcal/mol) accompanying with 4.8 kcal/mol energy intake. And the hydrogen bonding makes the energy barrier of loss N9−H slightly decrease.

The bp−H61−1 pathway was constructed to explore the potential of 8-oxoA$^{\bullet+}$:T deprotonation from N6−H1, which could be achieved in free 8-oxoA$^{\bullet+}$ along the H61−1 pathway. Due to the presence of the T base, W5′ coordinates to the O4 of the T base in Int33, where W6′ links with W5′ and directs to bulk water (Figure 7A). With this hydration model, an intact deprotonation of 8-oxoA$^{\bullet+}$:T could be probed, where

https://doi.org/10.1021/acsomega.4c08956
ACS Omega 2024, 9, 50730−50741

accompanying with the increase of N6···H1 distance, both TS13 and Int34 were captured. W3′ plays the role of proton bridge by forming H_3O^+, which then migrates to W5′ in Int34. The forward energy barrier of PT to adjacent water is 8.9 kcal/mol, which is endothermic, 10.6 kcal/mol (Figure 7B). It could be stabilized by PT to bulk water, forming pure 8-oxoA-(−H61)$^\bullet$:T (Int35) and the dissociation of coordinated water to sole 8-oxoA(−H61)$^\bullet$:T. The calculated results reveal that both the energy barrier and thermodynamics are lower than the case in free 8-oxoA$^{\bullet+}$, further verifying the influence of base pairing T on the reaction.

In order to disclose the possibility of PT toward N7, the hydration model of bp−H61−2 was built, which was adopted in the H61−2 pathway for free 8-oxoA$^{\bullet+}$. As with free 8-oxoA$^{\bullet+}$, the migration of N6−H1 toward the direction of N7 is infeasible, confirmed by the energy scan of N6−H1 bond (Figure 7C).

As mentioned above, the N6−H2 of 8-oxoA$^{\bullet+}$ in base pair is hydrogen bonding with O4 of T base different from free 8-oxoA$^{\bullet+}$. Generally, this may incur the PT to O4 of pairing T following the deprotonation from protonated T to form neutral radical as G$^{\bullet+}$ in GC base pair.[57] However, the PT of N6−H2 to neighboring T is inaccessible due to the absence of stable product. The profile of total energy scan for N6−H2 bond is exhibited in Figure 7D implying the result. It is evident that the hydrogen bonding inhibits the PT consistent with previous studies in other DNA bases.[18,28,42]

Now, a whole picture of 8-oxoA$^{\bullet+}$ deprotonation in a base pair can be exhibited. Except for N6−H2, the loss of other active protons from 8-oxoA$^{\bullet+}$ is possible as the reachable energy barrier, which is 1.3, −0.6, 3.3, and 8.9 in bp−H7−1, bp−H9−1, bp−H9−2, and bp−H61−1 pathways, respectively (Scheme 3). Obviously, the stepwise PT from N9 to adjacent water is also the most favorable pathway to form a neutral radical rather than direct deprotonation of N9−H and N7−H. This agrees well with that in free 8-oxoA$^{\bullet+}$. Interestingly, the deprotonation N9−H in 8-oxoA$^{\bullet+}$:T base pair occurs along the bp−H9−2 pathway uncovering the profound effects of hydrogen bonding on 8-oxoA$^{\bullet+}$ deprotonation, which is inaccessible in free 8-oxoA$^{\bullet+}$ due to the proton localization at neighboring water of N9−H. The behavior of loss of free proton appears to be adjusted by hydrogen bonding, which is unusual in comparison with previous studies.[54] Otherwise, the proton escape from N6−H2 is inhibited as the insurmountable PT from N6 of 8-oxoA$^{\bullet+}$ and O4 of paired T reveals the effect of hydrogen bonding on the constrained proton. This has been mentioned often in previous studies.[18,41,42] Finally, it should be pointed out that the encumbered context has a negligible influence on the stability of neutral radical in a single-layer 8-oxoA:T base pair.

Scheme 3. Degradation of 8-oxoA$^{\bullet+}$ to 8-oxoA(-H)$^\bullet$ in a Base Pair via Different Pathways

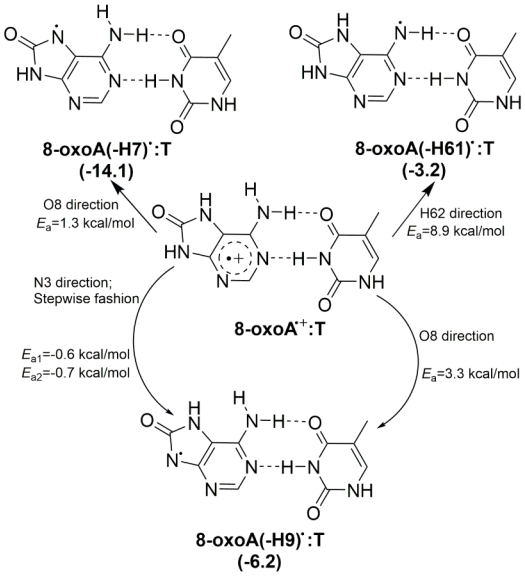

3. CONCLUSIONS

In this study, the deprotonation of 8-oxoA$^{\bullet+}$ in free and encumbered contexts was thoroughly investigated by DFT calculations. After carefully inspecting the calculated result, some insightful implications are summarized as follows:

(1) The preference of 8-oxoA$^{\bullet+}$ deprotonation is N9−H in both free and encumbered contexts, which is substituted by N7−H in real DNA due to the linkage between N9 and ribose. The calculated energy profiles reveal that the energy barrier of PT to adjacent water is rather low for N9−H and N7−H in both contexts, hinting at the feasibility of 8-oxoA$^{\bullet+}$ deprotonation from these two sites. The loss of proton from N6−H1 of 8-oxoA$^{\bullet+}$ could also occur but with increased energy barrier with respect to N9−H and N7−H. The deprotonation of N6−H2 proceeds in free 8-oxoA$^{\bullet+}$ with an energy barrier higher than these two imino protons, which is infeasible in a single-layer 8-oxoA:T base pair. Otherwise, the stability of the neutral radical also indicates the preference of 8-oxoA$^{\bullet+}$ deprotonation, which follows the order: 8-oxoA-(−H7)$^\bullet$ > 8-oxoA(−H9)$^\bullet$ > 8-oxoA(−H61)$^\bullet$ > 8-oxoA-(−H62)$^\bullet$ (absence in 8-oxoA:T base pair) in both contexts.

(2) A stepwise manner for PT of 8-oxoA$^{\bullet+}$ to adjacent water was observed. A previous study suggested that DNA radical cation (R) could initially migrate the active proton to neighboring water (TS) and then further transfer to adjacent water connecting with the water in a second hydration shell. The loss of an active proton to adjacent water is one step only. However, it is observed that the deprotonation N9−H of 8-oxoA$^{\bullet+}$ toward the direction of N3 follows a stepwise manner including proton localization at neighboring water and PT to adjacent water. It is unusual in comparison with previous studies.

(3) The behavior of the loss of free proton from 8-oxoA$^{\bullet+}$ could be influenced by hydrogen bonding. In free 8-oxoA$^{\bullet+}$, the N9−H is localized at neighboring water without further PT to adjacent water in the H9−2 pathway. However, the free N9−H could migrate directly to adjacent water in 8-oxoA$^{\bullet+}$:T base pair unraveling the influence of hydrogen bonding.

4. COMPUTATIONAL DETAILS

A previous study with 8-hydroxyguanine radical verified that the substitute at N9 with different groups has a negligible influence on the potential energy profiles.[49] Thus, 8-oxoA and a single-layer 8-oxoA:T base pair are chosen as the proper model for the calculations, where N9 of 8-oxoA and N1 of paired T are replaced with hydrogen. Indeed, the influence of ribose with syn- and anticonfiguration was also assessed, which only has a small effect on the energy barrier of 8-oxoA$^{\bullet+}$ deprotonation (Figure S6). Otherwise, a stacked 8-oxoA:T base pair was applied to disclose the stack effect on 8-oxoA$^{\bullet+}$:T

https://doi.org/10.1021/acsomega.4c08956
ACS Omega 2024, 9, 50730−50741

deprotonation. The energy barrier is higher than that obtained in a single-layer base pair (Figure S7), indicating the influence of base stacking on 8-oxoA$^{\bullet+}$:T deprotonation.

The method developed by Ho and Coote is used for the calculation of pK_a with some modifications, as described in our previous studies.[46,53] It should be noticed that the Gibbs free energy is obtained by optimizing the electronic structures of related species at the M06-2X/6-31+G(d,p) level of theory. The solvation effect is simulated by employing the integral equation formalism-polarized continuum model (IEFPCM) augmented with seven explicit water molecules. To obtain a reasonable pK_a value, the effects of solvation and other density functionals are also assessed, and the results are displayed in the Supporting Information. Since the triple-ξ basis set and the model with ribose do not have any obvious improvement for the calculation of pK_a,[46] the influence of basis set and ribose was not evaluated.

The electronic structure of related species involved in 8-oxoA$^{\bullet+}$ deprotonation was fully optimized at the M06-2X/6-31+G(d) level of theory, where IEFPCM combined with four explicit water molecules was used to imitate solvation effects. This method has been widely utilized to solve problems with respect to oxidative DNA damage.[29,36,46,54] And the numbers and roles of explicit water molecule were assessed (Figure S8), which is basically consistent with the case in guanine radical cation.[54] The identity of the stationary point and first-order saddle point (TS) is judged by vibrational frequency analysis obtained at the same theoretical level, where the initial intrinsic reaction coordinate (IRC) is performed to further confirm the exact connection of the respective minima. The single point energy of both stationary points and first-order saddle points is obtained at the IEFPCM/M06-2X/6-311++G(d,p) level of theory, which were presented after combining with the thermal correction to Gibbs free energy calculated at the IEFPCM/M06-2X/6-31+G(d) level of theory. All these calculations are performed with the Gaussian 16 suite of programs.[58]

■ ASSOCIATED CONTENT

Supporting Information

The Supporting Information is available free of charge at https://pubs.acs.org/doi/10.1021/acsomega.4c08956.

> Calculated pK_a of active proton in 8-oxoA and 8-oxoA$^{\bullet+}$ using other method and model; optimized geometries and Gibbs energy profiles of 8-oxoA$^{\bullet+}$ deprotonation using another model; the Cartesian coordinates for optimized structure (PDF)

■ AUTHOR INFORMATION

Corresponding Authors

Yinghui Wang − *College of Science, Chang'an University, Xi'an 710064, China;* orcid.org/0000-0001-7617-7433; Email: wangyinghui@chd.edu.cn

Simin Wei − *State Key Laboratory of Research & Development of Characteristic Qin Medicine Resources (Cultivation), Co-Construction Collaborative Innovation Center for Chinese Medicine Resources Industrialization by Shaanxi & Education Ministry, Shaanxi University of Chinese Medicine, Xianyang 712083, China;* orcid.org/0000-0001-9818-7595; Email: weismiccas@163.com

Author

Lei Ma − *College of Science, Chang'an University, Xi'an 710064, China*

Complete contact information is available at: https://pubs.acs.org/10.1021/acsomega.4c08956

Notes

The authors declare no competing financial interest.

■ ACKNOWLEDGMENTS

This work was financially supported by the National Natural Science Foundation of China (22103007, 82274353); Fundamental Research Funds for the Central Universities, CHD (300102124207); Key Research and Development Plan of Shaanxi Province (2024SF-YBXM-517, 2024SF-YBXM-426); Science and Technology Youth Stars Project of Shaanxi Province (2023KJXX-063); Science and Technology Innovation Talent System Construction Plan of Shaanxi University of Chinese medicine (2023-LJRC-03); Open Project of State Key Laboratory of Research and Development of Characteristic Qin Medicine Resources (SUCM-QM202207); and the Natural Science Foundation of Shaanxi Province (2024JC-YBQN-0586).

■ REFERENCES

(1) Warburton, R. E.; Soudackov, A. V.; Hammes-Schiffer, S. Theoretical Modeling of Electrochemical Proton-Coupled Electron Transfer. *Chem. Rev.* **2022**, *122* (12), 10599−10650.

(2) Huang, L.; Ji, T.; Zhu, C.; Yue, H.; Zhumabay, N.; Rueping, M. Bioinspired desaturation of alcohols enabled by photoredox proton-coupled electron transfer and cobalt dual catalysis. *Nat. Commun.* **2022**, *13* (1), 809.

(3) Zhong, J. Y.; Reinhardt, C. R.; Hammes-Schiffer, S. Role of Water in Proton-Coupled Electron Transfer between Tyrosine and Cysteine in Ribonucleotide Reductase. *J. Am. Chem. Soc.* **2022**, *144* (16), 7208−7214.

(4) Shi, Q. Q.; Pei, Z. P.; Song, J. S.; Li, S. J.; Wei, D. H.; Coote, M. L.; Lan, Y. Diradical Generation via Relayed Proton-Coupled Electron Transfer. *J. Am. Chem. Soc.* **2022**, *144* (7), 3137−3145.

(5) Agarwal, R. G.; Coste, S. C.; Groff, B. D.; Heuer, A. M.; Noh, H.; Parada, G. A.; Wise, C. F.; Nichols, E. M.; Warren, J. J.; Mayer, J. M. Free Energies of Proton-Coupled Electron Transfer Reagents and Their Applications. *Chem. Rev.* **2022**, *122* (1), 1−49.

(6) Murray, P. R. D.; Cox, J. H.; Chiappini, N. D.; Roos, C. B.; McLoughlin, E. A.; Hejna, B. G.; Nguyen, S. T.; Ripberger, H. H.; Ganley, J. M.; Tsui, E.; Shin, N. Y.; Koronkiewicz, B.; Qiu, G. Q.; Knowles, R. R. Photochemical and Electrochemical Applications of Proton-Coupled Electron Transfer in Organic Synthesis. *Chem. Rev.* **2022**, *122* (2), 2017−2291.

(7) Wang, F.; Stahl, S. S. Electrochemical Oxidation of Organic Molecules at Lower Overpotential: Accessing Broader Functional Group Compatibility with Electron-Proton Transfer Mediators. *Acc. Chem. Res.* **2020**, *53* (3), 561−574.

(8) Nocera, D. G. Proton-Coupled Electron Transfer: The Engine of Energy Conversion and Storage. *J. Am. Chem. Soc.* **2022**, *144* (3), 1069−1081.

(9) Golan, A.; Bravaya, K. B.; Kudirka, R.; Kostko, O.; Leone, S. R.; Krylov, A. I.; Ahmed, M. Ionization of dimethyluracil dimers leads to facile proton transfer in the absence of hydrogen bonds. *Nat. Chem.* **2012**, *4* (4), 323−329.

(10) Sauri, V.; Gobbo, J. P.; Serrano-Pérez, J. J.; Lundberg, M.; Coto, P. B.; Serrano-Andrés, L.; Borin, A. C.; Lindh, R.; Merchán, M.; Roca-Sanjuán, D. Proton/Hydrogen Transfer Mechanisms in the Guanine-Cytosine Base Pair: Photostability and Tautomerism. *J. Chem. Theory Comput.* **2013**, *9* (1), 481−496.

(11) Soler-Polo, D.; Mendieta-Moreno, J. I.; Trabada, D. G.; Mendieta, J.; Ortega, J. Proton Transfer in Guanine-Cytosine Base Pairs in B-DNA. *J. Chem. Theory Comput.* **2019**, *15* (12), 6984−6991.
(12) Srivastava, R. The Role of Proton Transfer on Mutations. *Front. Chem.* **2019**, *7*, 536.
(13) Palafox, M. A.; Pedraza Velasco, M. L. D.; Marín, J. I.; Posada-Moreno, P. How proton transfer affects the helical parameters in DNA: DNA microhelices. *J. Biomol. Struct. Dyn.* **2022**, *40* (24), 13759−13777.
(14) Koag, M. C.; Jung, H. M.; Lee, S. Mutagenesis mechanism of the major oxidative adenine lesion 7,8-dihydro-8-oxoadenine. *Nucleic Acids Res.* **2020**, *48* (9), 5119−5134.
(15) Koag, M. C.; Jung, H.; Lee, S. Mutagenic Replication of the Major Oxidative Adenine Lesion 7,8-Dihydro-8-oxoadenine by Human DNA Polymerases. *J. Am. Chem. Soc.* **2019**, *141* (11), 4584−4596.
(16) Chatgilialoglu, C.; Eriksson, L. A.; Krokidis, M. G.; Masi, A.; Wang, S. D.; Zhang, R. B. Oxygen Dependent Purine Lesions in Double-Stranded Oligodeoxynucleotides: Kinetic and Computational Studies Highlight the Mechanism for 5′,8-Cyclopurine Formation. *J. Am. Chem. Soc.* **2020**, *142* (12), 5825−5833.
(17) Banyasz, A.; Martínez-Fernández, L.; Balty, C.; Perron, M.; Douki, T.; Improta, R.; Markovitsi, D. Absorption of Low-Energy UV Radiation by Human Telomere G-Quadruplexes Generates Long-Lived Guanine Radical Cations. *J. Am. Chem. Soc.* **2017**, *139* (30), 10561−10568.
(18) Wang, Y. H.; Zhao, H. M.; Yang, C. F.; Jie, J. L.; Dai, X. J.; Zhou, Q.; Liu, K. H.; Song, D.; Su, H. M. Degradation of Cytosine Radical Cations in 2′-Deoxycytidine and in i-Motif DNA: Hydrogen-Bonding Guided Pathways. *J. Am. Chem. Soc.* **2019**, *141* (5), 1970−1979.
(19) Bielskute, S.; Plavec, J.; Podbevsek, P. Impact of Oxidative Lesions on the Human Telomeric G-Quadruplex. *J. Am. Chem. Soc.* **2019**, *141* (6), 2594−2603.
(20) Fleming, A. M.; Burrows, C. J. Chemistry of ROS-mediated oxidation to the guanine base in DNA and its biological consequences. *Int. J. Radiat. Biol.* **2022**, *98* (3), 452−460.
(21) Krokan, H. E.; Bjorås, M. Base Excision Repair. *Csh. Perspect. Biol.* **2013**, *5* (4), a012583.
(22) Servius, H. W.; Pidugu, L. S.; Sherman, M. E.; Drohat, A. C. Rapid excision of oxidized adenine by human thymine DNA glycosylase. *J. Biol. Chem.* **2023**, *299* (1), 1−11.
(23) Grin, I. R.; Dianov, G. L.; Zharkov, D. O. The role of mammalian NEIL1 protein in the repair of 8-oxo-7,8-dihydroadenine in DNA. *FEBS Lett.* **2010**, *584* (8), 1553−1557.
(24) Kruchinin, A. A.; Kamzeeva, P. N.; Zharkov, D. O.; Aralov, A. V.; Makarova, A. V. 8-Oxoadenine: A ≪New≫ Player of the Oxidative Stress in Mammals? *Int. J. Mol. Sci.* **2024**, *25* (2), 1342.
(25) Tew, D. J.; Hebert, J. M.; Schmier, B. J. Discovery and properties of a monoclonal antibody targeting 8-oxoA, an oxidized adenine lesion in DNA and RNA. *Redox Biol.* **2023**, *62*, 102658.
(26) Poetsch, A. R. The genomics of oxidative DNA damage, repair, and resulting mutagenesis. *Comput. Struct. Biotec.* **2020**, *18*, 207−219.
(27) Wang, Y. H.; Wei, S. M. Influence of hydrogen bonds on the reaction of guanine and hydroxyl radical: DFT calculations in C(H^+)GC motif. *Phys. Chem. Chem. Phys.* **2024**, *26* (6), 5683−5692.
(28) Wei, S.; He, Q.; Duan, J.; Zheng, H.; Ma, L.; Wang, Y. An Exploration of the Transformation of the 8-Oxo-7,8-Dihydroguanine Radical Cation to Protonated 2-Amino-5-Hydroxy-7,9-Dihydropurine-6,8-Dione in a Base Pair. *ChemPhyschem* **2023**, *24* (3), No. e202200625.
(29) Wang, Y. H.; Wei, S. M. Theoretical insights into the reaction mechanism of hydroxyl radicals and guanine in G-quadruplex DNA. *Phys. Chem. Chem. Phys.* **2023**, *25* (23), 16126−16134.
(30) Moe, M. M.; Benny, J.; Liu, J. B. Collision-induced dissociation of homodimeric and heterodimeric radical cations of 9-methylguanine and 9-methyl-8-oxoguanine: Correlation between intra-base pair proton transfer originating from the N1-H at a Watson-Crick edge and non-statistical dissociation. *Phys. Chem. Chem. Phys.* **2022**, *24* (16), 9263−9276.
(31) Yinghui, W.; Haoming, X.; Bin, M.; Zongxuan, L.; Yating, M.; Lei, M.; Simin, W. Theoretical Studies of Effect of Hydrogen Bond on Reaction of Hydroxyl Radicals and Guanine. *Chem. J. Chin. Univ.* **2024**, *45* (8), 20240208.
(32) Zheng, L. W.; Greenberg, M. M. DNA Damage Emanating From a Neutral Purine Radical Reveals the Sequence Dependent Convergence of the Direct and Indirect Effects of γ-Radiolysis. *J. Am. Chem. Soc.* **2017**, *139* (49), 17751−17754.
(33) Robert, G.; Wagner, J. R.; Cadet, J. Oxidatively generated tandem DNA modifications by pyrimidinyl and 2-deoxyribosyl peroxyl radicals. *Free Radical Bio. Med.* **2023**, *196*, 22−36.
(34) Andrés, C. M. C.; de la Lastra, J. M. P.; Juan, C. A.; Plou, F. J.; Pérez-Lebeña, E. Chemical Insights into Oxidative and Nitrative Modifications of DNA. *Int. J. Mol. Sci.* **2023**, *24* (20), 15240.
(35) Matter, B.; Seiler, C. L.; Murphy, K.; Ming, X.; Zhao, J. W.; Lindgren, B.; Jones, R.; Tretyakova, N. Mapping three guanine oxidation products along DNA following exposure to three types of reactive oxygen species. *Free Radical Bio. Med.* **2018**, *121*, 180−189.
(36) Wang, Y. H.; Wei, S. M.; Wang, K.; Xu, R. R.; Zhao, H. M. A Theoretical Study of 8-Azaguanine Radical Cation Deprotonation. *Acta Chim. Sin.* **2020**, *78* (3), 271−278.
(37) Shinde, S. S.; Maroz, A.; Hay, M. P.; Anderson, R. F. One-Electron Reduction Potential of the Neutral Guanyl Radical in the GC Base Pair of Duplex DNA. *J. Am. Chem. Soc.* **2009**, *131* (14), 5203−5207.
(38) Wang, Y.; Liu, L. L.; Gao, Y.; Zhao, J. Y.; Liu, C.; Gong, L. D.; Yang, Z. Z. Development of a QM/MM(ABEEM) method for the deprotonation of neutral and cation radicals in the G-tetrad and GGX(8-oxo-G) tetrad. *Phys. Chem. Chem. Phys.* **2023**, *26* (1), 504−516.
(39) Kumar, A.; Adhikary, A.; Sevilla, M. D.; Close, D. M. One-electron oxidation of ds(5′-GGG-3′) and ds(5′-G(8OG)G-3′) and the nature of hole distribution: A density functional theory (DFT) study. *Phys. Chem. Chem. Phys.* **2020**, *22* (9), 5078−5089.
(40) Sosorev, A.; Kharlanov, O. Organic nanoelectronics inside us: Charge transport and localization in RNA could orchestrate ribosome operation. *Phys. Chem. Chem. Phys.* **2021**, *23* (12), 7037−7047.
(41) Wu, L. D.; Liu, K. H.; Jie, J. L.; Song, D.; Su, H. M. Direct Observation of Guanine Radical Cation Deprotonation in G-Quadruplex DNA. *J. Am. Chem. Soc.* **2015**, *137* (1), 259−266.
(42) Wang, Y. H.; Zhao, H. M.; Zhou, Q.; Dai, X. J.; Liu, K. H.; Song, D.; Su, H. M. Monitoring the Structure-Dependent Reaction Pathways of Guanine Radical Cations in Triplex DNA: Deprotonation Versus Hydration. *J. Phys. Chem. B* **2019**, *123* (13), 2853−2863.
(43) Wang, Y. H.; Jie, J. L.; Zhao, H. M.; Bai, Y.; Qin, P. X.; Song, D. Deprotonation of Guanine Radical Cation in G-Quadruplex: A Combined Experimental and Theoretical Study. *Acta Chim. Sin.* **2018**, *76* (6), 475−482.
(44) Kumar, A.; Sevilla, M. D. Proton-Transfer Reactions in One-Electron-Oxidized G-Quadruplexes: A Density Functional Theory Study. *J. Phys. Chem. B* **2022**, *126* (7), 1483−1491.
(45) Karwowski, B. T. The Influence of Oxidized Imino-Allantoin in the Presence of ^{OXO}G on Double Helix Charge Transfer: A Theoretical Approach. *Int. J. Mol. Sci.* **2024**, *25* (11), 5962.
(46) Wei, S. M.; Zhang, Z. H.; Liu, S. J.; Wang, Y. H. Theoretical insight into 7,8-dihydrogen-8-oxoguanine radical cation deprotonation. *New J. Chem.* **2021**, *45* (25), 11202−11212.
(47) Shafirovich, V.; Cadet, J.; Gasparutto, D.; Dourandin, A.; Huang, W. D.; Geacintov, N. E. Direct spectroscopic observation of 8-oxo-7,8-dihydro-2′-deoxyguanosine radicals in double-stranded DNA generated by one-electron oxidation at a distance by 2-aminopurine radicals. *J. Phys. Chem. B* **2001**, *105* (2), 586−592.
(48) Fleming, A. M.; Muller, J. G.; Dlouhy, A. C.; Burrows, C. J. Structural Context Effects in the Oxidation of 8-Oxo-7,8-dihydro-2′-deoxyguanosine to Hydantoin Products: Electrostatics, Base Stacking, and Base Pairing. *J. Am. Chem. Soc.* **2012**, *134* (36), 15091−15102.

https://doi.org/10.1021/acsomega.4c08956
ACS Omega 2024, 9, 50730−50741

(49) Munk, B. H.; Burrows, C. J.; Schlegel, H. B. An exploration of mechanisms for the transformation of 8-oxoguanine to guanidinohydantoin and spiroiminodihydantoin by density functional theory. *J. Am. Chem. Soc.* **2008**, *130* (15), 5245−5256.
(50) Choi, Y. J.; Chang, S. J.; Gibala, K. S.; Resendiz, M. J. E. 8-Oxo-7,8-dihydroadenine and 8-Oxo-7,8-dihydroadenosine Chemistry, Structure, and Function in RNA and Their Presence in Natural Products and Potential Drug Derivatives. *Chem.—eur. J.* **2017**, *23* (28), 6706−6716.
(51) Ravanat, J. L.; Guicherd, P.; Tuce, Z.; Cadet, J. Simultaneous determination of five oxidative DNA lesions in human urine. *Chem. Res. Toxicol.* **1999**, *12* (9), 802−808.
(52) Singh, T. A.; Rao, B. S. M.; O'Neill, P. Radical Chemistry of 8-Oxo-7,8-dihydro-2′-deoxyadenosine and 8-Oxo-7,8-dihydro-2′-deoxyguanosine: A Pulse Radiolysis Study. *J. Phys. Chem. B* **2010**, *114* (49), 16611−16617.
(53) Thapa, B.; Schlegel, H. B. Calculations of pK_a's and Redox Potentials of Nucleobases with Explicit Waters and Polarizable Continuum Solvation. *J. Phys. Chem. A* **2015**, *119* (21), 5134−5144.
(54) Zhang, X. W.; Jie, J. L.; Song, D.; Su, H. M. Deprotonation of Guanine Radical Cation $G^{\bullet+}$ Mediated by the Protonated Water Cluster. *J. Phys. Chem. A* **2020**, *124* (29), 6076−6083.
(55) Kumar, A.; Sevilla, M. D. Influence of Hydration on Proton Transfer in the Guanine-Cytosine Radical Cation ($G^{\bullet+}$-C) Base Pair: A Density Functional Theory Study. *J. Phys. Chem. B* **2009**, *113* (33), 11359−11361.
(56) Marx, D.; Tuckerman, M. E.; Hutter, J.; Parrinello, M. The nature of the hydrated excess proton in water. *Nature* **1999**, *397* (6720), 601−604.
(57) Cerón-Carrasco, J. P.; Requena, A.; Perpète, E. A.; Michaux, C.; Jacquemin, D. Theoretical Study of the Tautomerism in the One-Electron Oxidized Guanine-Cytosine Base Pair. *J. Phys. Chem. B* **2010**, *114* (42), 13439−13445.
(58) Frisch, M. J.; Schlegel, G. W. T. H. B.; Scuseria, G. E.; Robb, M. A.; Cheeseman, J. R.; Scalmani, G.; Barone, V.; Petersson, G. A.; Nakatsuji, H.; Li, X., et al. *Gaussian 16 (Revision A.03)*; Fox, D. J., Ed.; Gaussian, Inc: Wallingford CT, 2016.

https://doi.org/10.1021/acsomega.4c08956
ACS Omega 2024, 9, 50730−50741